Enhanced magnetic dichroism in dark-field UV photoemission electron microscopy

Maximilian Paleschke,[1] David Huber,[1] Friederike Wührl,[1] Cheng-Tien Chiang,[2] Frank O. Schumann,[3] Jürgen Henk,[1] and Wolf Widdra[1,*]

[1]*Institute of Physics, Martin Luther University, Halle-Wittenberg, D-06099 Halle (Saale), Germany*
[2]*Institute of Atomic and Molecular Sciences, Academia Sinica, Taipei, Taiwan*
[3]*Max-Planck-Institut für Mikrostrukturphysik, D-06120 Halle, Germany*

(Received 7 September 2024; revised 15 May 2025; accepted 14 July 2025; published 4 August 2025)

Photoemission electron microscopy (PEEM) has evolved into an indispensable tool for structural and magnetic characterization of surfaces at the nanometer scale. In strong contrast to synchrotron-radiation-based x-ray PEEM as a leading method for element-specific magnetic properties via magnetic circular dichroism (MCD), laboratory ultraviolet (UV) PEEM has seen limited application with much smaller dichroic effects for in-plane magnetization. Here, we introduce dark-field PEEM as an approach to enhance MCD contrast in threshold photoemission, enabling efficient MCD imaging with significantly enhanced contrast by an order of magnitude for Fe(001). This advancement paves the way for MCD imaging on femtosecond timescales using modern lasers. The experimental results will be quantitatively benchmarked against advanced relativistic photoemission calculations.

DOI: 10.1103/klc4-lk7g

I. INTRODUCTION

Ultrafast spin and magnetization dynamics are rapidly growing fields in condensed matter physics, holding great promise for both fundamental research and future device applications. Ultrafast imaging of magnetic domains on the micrometer scale is well established using all-optical methods, such as magneto-optical Kerr microscopy, which is inherently limited by optical diffraction. Alternatively, ultrafast scanning tunneling microscopy (STM) offers spatial resolution down to the atomic scale. However, its sensitivity to electron spin dynamics at surfaces depends on the spin-polarized current from the tip [1], and the recent development of ultrafast STM using THz electric fields [2] only provides the spin information if spin-orbit split electronic states can be probed in the tunneling process [3]. In contrast, the combination of ultrafast lasers with the Lorentz transmission electron microscopy can offer the direct magnetic contrast in the femtosecond time domain in the transmitted volume [4–6].

To access the surface-sensitive magnetization dynamics, magnetic circular dichroism (MCD) provides a known contrast mechanism used for imaging magnetic domains in photoelectron emission microscopy (PEEM). The intensity recorded for a particular domain changes with the helicity of the incident radiation, thereby producing magnetic contrast without the need for explicitly detecting the electron spin. By tuning the incident x-ray radiation to a magnetic core level absorption edge, substantial and element-specific MCD asymmetries have been reported. With the wide availability of tunable synchrotron radiation, this technique of XMCD-PEEM is well established for magnetic domain imaging on the nanometer scale [7]. However, the pulse length of synchrotron radiation of typically 30–50 ps renders XMCD-PEEM unsuitable on ultrafast timescales. The reduced pulse length of x-ray free-electron lasers (XFELs) can solve this issue [8]. However, the general availability is lower than for laboratory-based experiments. Lower pulse repetition rates and time-restricted beamtimes of the XFEL limit available photoemission statistics. Here, we have combined PEEM with the MHz repetition rates of a high-power laser system as well as a Hg discharge lamp, thereby minimizing the space-charge effects and allowing extended experiments in the laboratory. UV laser sources excite electrons from close to the Fermi level to energies slightly above the escape threshold. The reported MCD contrasts, especially for in-plane magnetization, are so small in threshold photoemission [9] that UV-PEEM has been discarded for magnetic domain imaging in the last two decades. Obviously, magnetic contrast needs to be increased for domain imaging with ultrashort laser pulses.

As we demonstrate here, the concept of dark-field PEEM in threshold photoemission allows efficient MCD imaging with an order-of-magnitude enhanced MCD contrast for in-plane magnetization. It paves the way for MCD imaging on femtosecond timescales with modern UV laser sources. Dark-field PEEM imaging uses an aperture for photoelectron momentum selection in the back focal plane of the electron imaging column prior to forming the real-space image. We will demonstrate this for the in-plane magnetic structure at the Fe(001) surface and compare quantitatively the experimental results with fully relativistic photoemission calculations.

*Contact author: wolf.widdra@physik.uni-halle.de

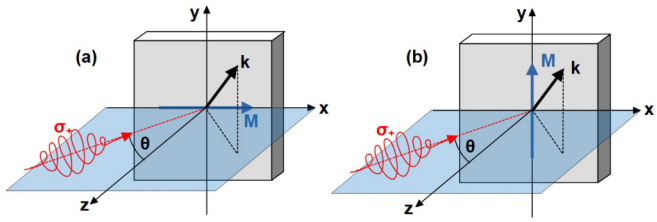

FIG. 1. Symmetry analysis. A circularly polarized laser pulse (shown in red, with helicity σ_+) impinges onto a magnetic domain (rectangular solid). The light incidence direction and the surface normal (z axis) span the scattering plane (blue; xz-plane) with the magnetization direction $\boldsymbol{M}$ oriented within (a) or perpendicular (b) to the scattering plane, respectively. The off-normal detection of photoelectrons with wave vector $\boldsymbol{k}$ (black arrow) results in a chiral setup.

Following initial reports of magnetic dichroism in UV photoemission and its theoretical description in the 1990s [10–12], Marx *et al.* reported the first observation of magnetic dichroism in threshold PEEM in 2000 [9]. This study of polycrystalline Fe revealed an asymmetry in magnetic linear dichroism of 0.37%. Subsequent spectroscopic studies confirmed the presence of both circular and linear dichroism in various ferromagnetic materials. Building on Marx's experimental work, Nakagawa *et al.* studied Ni films adsorbed with Cs and discovered significant asymmetries of up to 12% in circular dichroism PEEM for out-of-plane magnetized domains [13–16]. This work also demonstrated the feasibility of using pulsed laser light for dichroism imaging. However, due to the limited photon energy range of common optical laser setups, Cs remained necessary in most photoemission experiments in order to reduce the work function [17,18], although PEEM studies using a deep-UV laser with a photon energy of 7 eV have been reported [19].

The theoretical framework for valence-band dichroism was primarily developed in the 1990s and early 2000s [11,12,20–25] and was bolstered by pioneering experiments [26–29]. It is based on calculating the relativistic electronic structures in conjunction with a theoretical description of the photoemission process. The extension of this description to threshold photoemission predicted that experimentally accessible magnetic dichroism levels are expected [22].

II. CONCEPTUAL BASIS

For a simplified conceptual approach, we consider a surface with fourfold symmetry, as e.g., the (001) fcc or bcc surfaces with magnetic easy axes along one of the four [100] or [110] directions. Let us assume light incidence along the surface normal (the case of $\theta = 0$ in Fig. 1). The photoemission intensity of electrons detected with off-normal wave vector $\boldsymbol{k}$ depends then on the helicity, σ_+ or σ_-, of the incident circularly polarized laser radiation and on the two orientations $\pm M$ of the in-plane magnetization in a selected domain, yielding four intensities $I_{\boldsymbol{k}}(\sigma_\pm, \pm M)$ (shortened $I_{\pm\pm}$). The latter intensities are combined into the total intensity

$$I \equiv I_{++} + I_{+-} + I_{-+} + I_{--}. \tag{1}$$

In order to disentangle the two main contrast mechanisms, we define appropriate asymmetries [30],

$$A_{\rm pol} \equiv [(I_{++} + I_{+-}) - (I_{-+} + I_{--})]/I, \tag{2a}$$

$$A_{\rm ex} \equiv [(I_{++} + I_{--}) - (I_{+-} + I_{-+})]/I. \tag{2b}$$

In the polarization asymmetry $A_{\rm pol}$ the magnetization's orientation is averaged out; it thus encodes contrast due to the light's helicity, as if the domain were nonmagnetic. Contrast due to the exchange splitting is quantified by the exchange asymmetry $A_{\rm ex}$, in which one averages over the mutual orientations of helicity and magnetization. Note that the *chiral geometry* for photoelectrons with *off-normal* wave vector $\boldsymbol{k}$ outside the scattering plane results in magnetic dichroism and, hence, in magnetic contrast.

If the scattering plane is a mirror plane of the lattice, the photoemission intensities for fixed $\boldsymbol{k}$ within the scattering plane obey $I_{++} = I_{--}$ for a magnetization within the scattering plane [Fig. 1(a)]. This results in a nonzero $A_{\rm ex}$ for $\boldsymbol{k} \neq \boldsymbol{0}$, but vanishing $A_{\rm pol}$. For magnetization perpendicular to the scattering plane, $I_{++} = I_{-+}$ holds that leads to vanishing $A_{\rm pol}$ and vanishing $A_{\rm ex}$.

III. THEORETICAL AND EXPERIMENTAL SETUP

In the following, we compare experimental results for a photon energy of 5.2 eV with theoretical MCD asymmetries based on relativistic photoemission computations for Fe(001) using the computer program package OMNI. The latter is based on the spin-polarized relativistic layer Korringa-Kohn-Rostoker (layer-KKR) method as applied earlier, e.g., in Ref. [31] and references therein. The sample is taken as semi-infinite Fe(100).

Self-consistent electronic-structure calculations have been performed using the local spin-density approximation for the exchange-correlation functional in density-functional theory. For solving the single-site scattering problem, the layer-KKR method uses an expansion of the scattering solutions with respect to angular momentum, in this work up to $l_{\rm max} = 3$. The potentials of the seven outermost layers of the semi-infinite system differ from that of the remainder (bulk). The interlayer scattering relies on a plane-wave expansion, here with at least 45 plane waves. For the image-potential barrier we take a smooth shape described in Ref. [32]. The calculated bulk and the surface electronic structures as well as the layer-resolved magnetic moments agree with those computed and published elsewhere.

The results of the electronic-structure calculations serve as the basis for the spin- and angle-resolved photoemission calculations, for which the same potentials as for the electronic-structure calculations are used. The spin-polarized photocurrent is calculated within the one-step model of photoemission, taking a time-reversed low-energy electron diffraction (LEED) state as final state. Photoelectrons excited within the topmost 50 layers are considered in order to obtain converged intensities and spin polarizations. The calculated spin-density matrix of the photoelectron allows to derive all components of the photoelectron's spin polarization vector.

The experimental photocurrent has been recorded for 65° grazing light incidence within the [100] high-symmetry direc-

tion in a standard PEEM setup (Focus GmbH, Hünstetten). As a light source either a mercury discharge lamp or the frequency-doubled output of a noncollinear optical amplifier (NOPA) with circular polarization optics is used [33–35]. The Fe(001) surface has been prepared by standard surface science procedures (as sputtering and annealing) and confirmed by low-energy electron diffraction and Auger or x-ray photoelectron spectroscopy.

IV. CONTRAST MECHANISMS

The $\boldsymbol{k}_{\parallel}$-dependent pattern of the polarization asymmetry A_{pol}, defined in Eq. (2a) and depicted in Fig. 2, depends on the binding energy of the initial states. Both experimental (left column) and theoretical data (right column) show that this contrast mechanism is sizable with absolute values up to about 20% in experiment and 40% in theory; it can thus hardly be ignored.

The theoretical pattern in the momentum space (right column in Fig. 2) exhibits a nodal line at $k_y = 0$ and a nodal line at almost $k_x = 0$. Moreover, one finds a change of sign if k_y is reversed. These features are imposed by the symmetry of the setup. Note that an antisymmetric pattern with respect to the $k_x = 0$ *and* $k_y = 0$ lines follows strictly only for normal light incidence [36]. However, the breaking of the antisymmetric behavior with respect to the $k_x = 0$ line due to the off-normal light incidence is hardly visible. The experimental data (left column) display the same features, and the overall agreement between experiment and theory is remarkably good, which includes also the sign change for binding energies above and below 0.2 eV. Note that the experimental asymmetries have been determined from two independent sets of two-dimensional (2D) momentum maps for magnetization directions $+\boldsymbol{M}$ and $-\boldsymbol{M}$ oriented along the $+x$ and $-x$ directions, respectively, via selection of appropriate individual magnetic domains.

The momentum-dependent exchange asymmetry A_{ex}, defined in Eq. (2b) and shown in Fig. 3, exhibits absolute values up to 10% in theory and 6% in experiment, which are an order-of-magnitude stronger effects than previously observed [9]. An odd symmetry of the momentum-dependent A_{ex} pattern with respect to the $k_x = 0$ line would be expected for normal light incidence [36]. However, for the grazing light incidence here, we find a clear deviation, which results in a curved nodal line between the regions of positive and negative A_{ex}. With respect to the $k_y = 0$ line, both experiments and theoretical calculations show a mirror-symmetric pattern in contrast to A_{pol}. The absolute A_{ex} values, including the sign, depend on the initial state binding energy via the band structure and photoemission matrix elements.

The above findings support that both asymmetries A_{pol} and A_{ex} are suitable tools for disentangling and quantifying available contrast mechanisms for dark-field domain imaging.

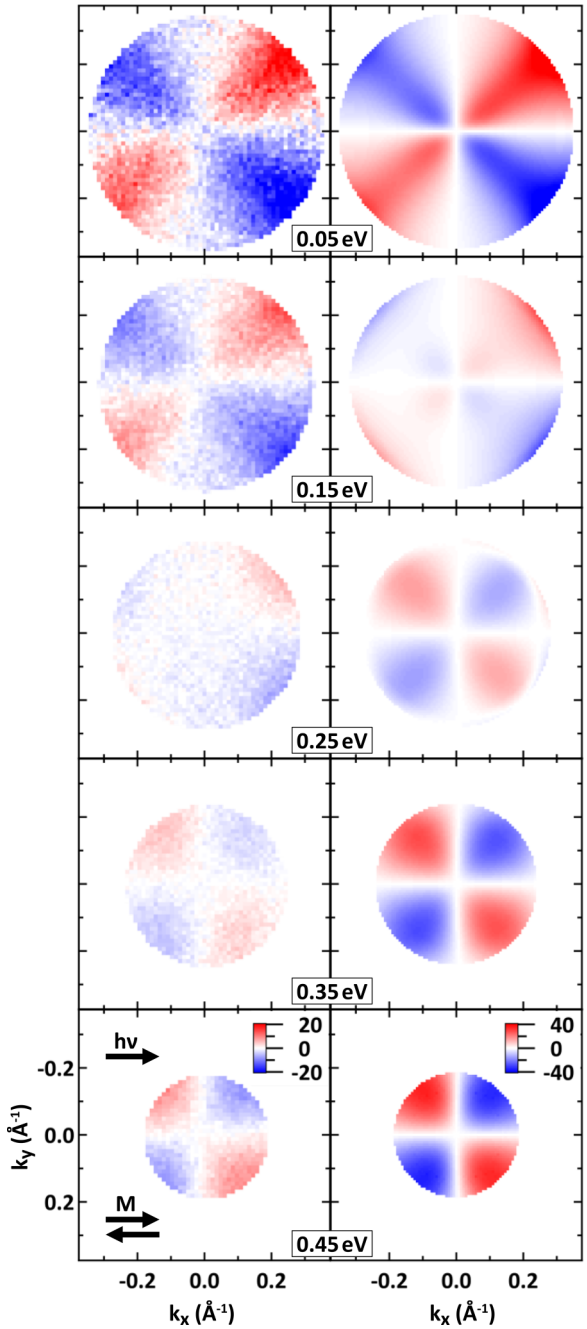

FIG. 2. Momentum-resolved polarization asymmetry A_{pol} of Fe(001) at selected binding energies for 65° grazing light incidence. Left column: Experimental results. The arrow marked $h\nu$ indicates the light incidence direction. The arrows M represent the two magnetization directions considered for A_{pol}. Right column: Respective theoretical results obtained from photoemission calculations. The binding energy is indicated at each panel. The color scale, showing A_{pol} as defined in Eq. (2a) in percent, is identical for all panels in a column.

V. DOMAIN IMAGING

From the momentum-resolved A_{ex} pattern in Fig. 3, it follows that MCD imaging can selectively reveal strong magnetic contrast in the case of *off-normal* electron momentum selection. However, without momentum selection or with a momentum selection centered at $k_x = k_y = 0$, which has been conventionally applied in the literature, different in-plane momentum contributions will largely cancel each other. This cancellation explains the small or vanishing magnetic dichroism for in-plane magnetized domains reported so far.

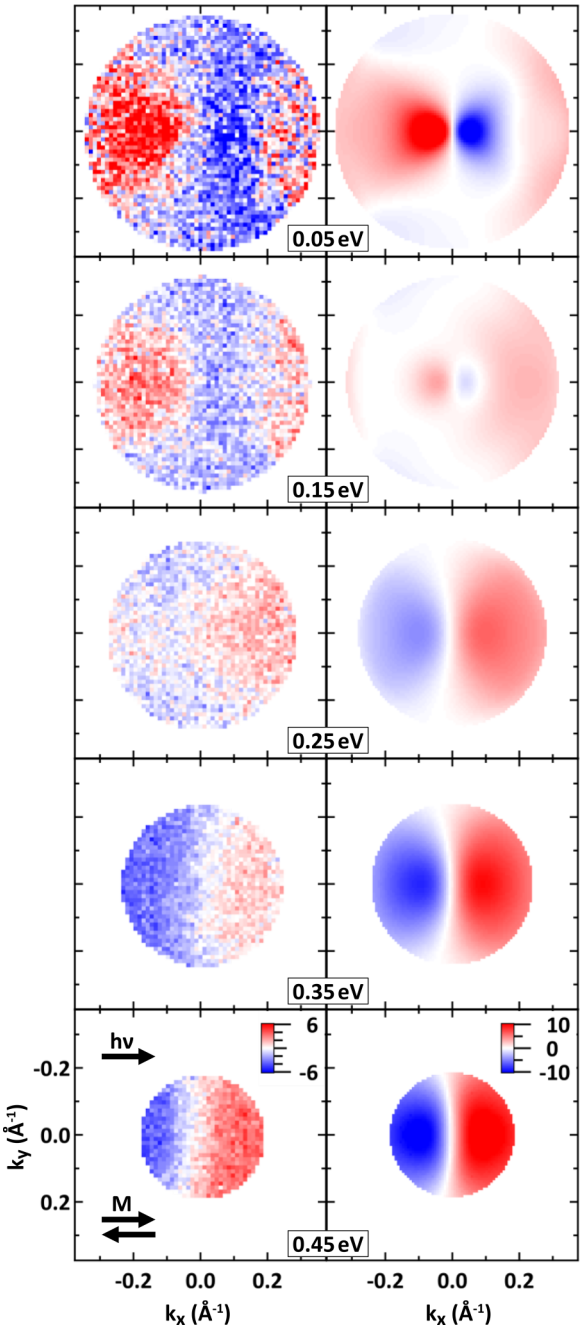

FIG. 3. Momentum-resolved exchange asymmetry A_{ex} of Fe(001) at selected binding energies, as in Fig. 2. Left column: Experimental PEEM data. Right column: Respective data from photoemission calculations. Small differences with respect to an odd symmetry upon reversal of k_x result from off-normal light incidence. For normal incidence they are absent.

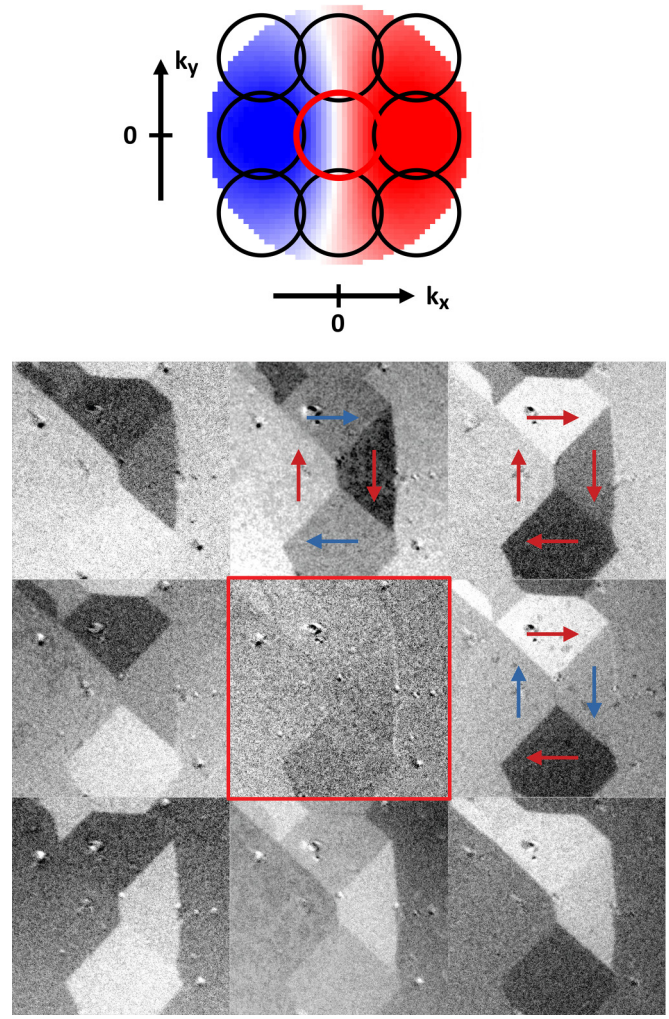

FIG. 4. Dark-field MCD imaging of Fe(100). Top: Schematics of the nine aperture positions in the momentum plane, with a momentum-resolved A_{ex} pattern as the background. Bottom: Domain imaging using the nine aperture positions shown above. ($h\nu$ = 5.2 eV, maximum domain contrast is between 3% and 4%, field of view 56 × 56 μm^2 each.)

Our joint experimental and theoretical study suggests to selectively choose the $\boldsymbol{k}_\parallel$ area of interest in order to enhance the magnetic contrast. Hence, we place a circular contrast aperture in a $\boldsymbol{k}_\parallel$ area with high exchange asymmetry, a procedure known as dark-field imaging in optics and modern electron microscopy.

Depending on the position of the aperture the contrast of specific domains is increased, as we show for a Landau-like pattern of four orthogonal magnetic domains at a Fe(001) surface (Fig. 4). Placing the aperture in nine different positions (shown as circles in the top panel of Fig. 4) results in nine corresponding MCD PEEM images of the same surface region (bottom panel).

For the centered aperture, marked in red, the MCD contrast almost vanishes in accordance with our above discussion. However, an aperture centered at $k_x > 0$ and $k_y = 0$ results in a drastically increased contrast of 3%–4% for magnetic domains oriented in the $+x$ vs $-x$ direction, whereas the contrast for domains oriented in the $+y$ and $-y$ directions (blue arrows) vanishes. Both observations match quantitatively the result of the $\boldsymbol{k}_\parallel$ space measurements in Fig. 3.

Positioning the momentum aperture at $k_x < 0$ and $k_y = 0$ reverses the contrast of $+x$ and $-x$ domains. As expected, the contrast switches from sensitivity in the x direction to the y direction when positioning the aperture at $k_x = 0$ and $k_y > 0$ (upper-middle PEEM image in Fig. 4). The upper-

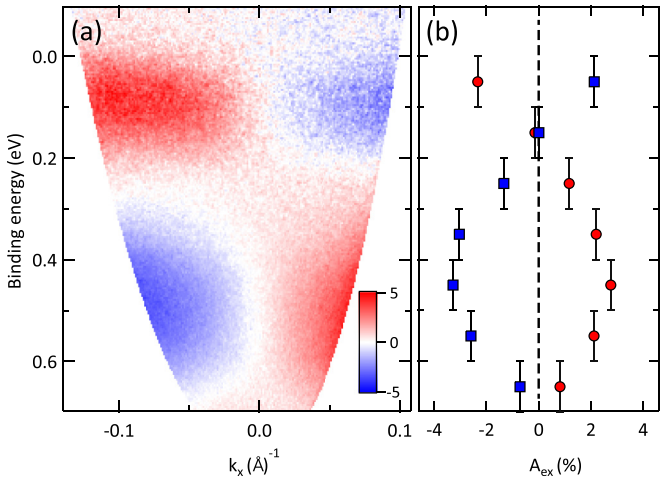

FIG. 5. Binding-energy-dependent exchange asymmetry A_{ex} for Fe(001)-(1 × 1)-O at $h\nu = 5.2$ eV. (a) ARPES data for an oxygen-passivated Fe(001) thin film grown on MgO(001) with the sample magnetized in the $+x$ and $-x$ direction (light incidence at 70°, $k_y = 0$). (b) Momentum-selected PEEM data for an oxygen-passivated Fe(001) single crystal for positive and negative k_x momentum selection as marked by blue squares and red circles, respectively. [Selection at $|k_x| = (0.16 \pm 0.12)$ Å^{-1}, $k_y = (0 \pm 0.12)$ Å^{-1}, light incidence at 65 °.]

right measurement shows a diagonal position with $k_x > 0$ and $k_y > 0$, where the different contributions to the MCD signal are combined, resulting in four different asymmetry values for the four in-plane magnetization directions. Note that in the latter case, besides A_{ex}, A_{pol} could also contribute to the domain contrasts, however, which is negligible here [36].

VI. INITIAL-STATE EFFECTS

The magnitude of A_{ex} and, therefore, of the MCD contrast in PEEM for near-threshold photoemission depend on the initial-state energy, as is demonstrated in Fig. 3. A_{ex} reverses sign from up to +6 % slightly below the Fermi level to −4 % at $E_B = 0.45$ eV. As a second, magnetically similar system we studied the oxygen-passivated Fe(001)-(1 × 1)-O surface with dark-field threshold PEEM, as described above. It yields very similar A_{pol} and A_{ex} patterns as those for bare Fe(001) (not shown here), which reverse sign at a binding energy of approximately 0.2 eV. Momentum-selected A_{ex} data from momentum-resolved PEEM measurements on the two magnetized domains in the $\pm x$ direction are shown in Fig. 5(b) for positive k_x as blue squares and for negative k_x as red circles.

Using an angle-resolved photoelectron spectroscopy (ARPES) setup described previously [34,37], the magnetic circular dichroism is analyzed in an independent experiment with higher-energy resolution for an 11-nm-thick Fe(001)-(1 × 1)-O thin film grown on MgO(001). For films magnetized fully in the $+x$ or $-x$ direction, the exchange asymmetry A_{ex} is depicted in an energy versus momentum map in Fig. 5(a). Note that the acceptance angle of the ARPES spectrometer is limited to ±15°. Both datasets show large A_{ex} values, which switch sign upon reversal of k_x. At the Fermi level and at $E_B = 0.45$ eV we find a strong contrast of about 5% between A_{ex} values of +2% and −3% with a

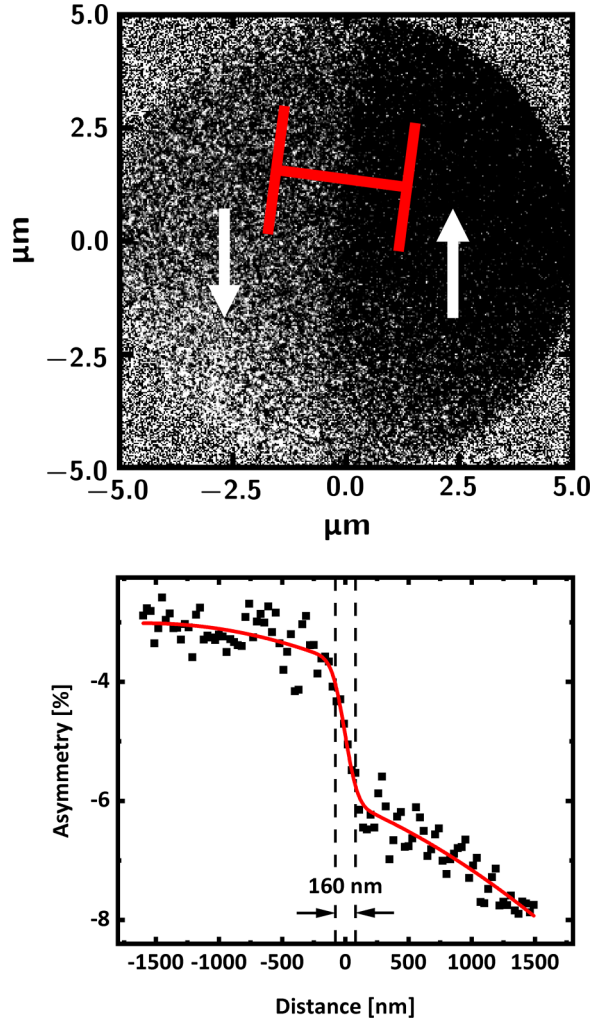

FIG. 6. Dark-field MCD imaging of an oxygen-passivated Fe(001) thin film grown on MgO(001) with a field of view of 10 × 10 µm^2. The linescan along the indicated red line shows an apparent domain wall width of 160 nm. The solid line indicates a fit using a Gaussian error function on a quadratic background. Laser photon energy of 4.66 eV, acquisition time 500 s.

contrast reversal between 0.15 and 0.25 eV. We note that this observation requires either precise threshold photoexcitation or energy-resolved electron detection to achieve high MCD signals. These spectroscopic observations, together with our microscopy data, demonstrate that the full energy-momentum phase space of electronic states, even for paradigmatic systems such as Fe, can be fully utilized for magnetic dichroic domain imaging.

While the dark-field scheme of threshold MCD PEEM is broadly applicable, the magnitude of the binding-energy-dependent exchange asymmetry A_{ex} is a material-specific property. It results from the spin-dependent electronic structure of Fe(001) and the associated ARPES transition matrix elements. Note that for a fixed binding energy these matrix elements depend on the photon energy due to the selective combination of the initial and final electronic states involved. Note further that our approach can be also implemented into momentum microscopy [38], where the original development

stems from back focal plane imaging in a photoelectron microscope [39].

A representative spatial resolution achieved in PEEM-based magnetic imaging is demonstrated in Fig. 6 for the Fe(001) thin film grown on MgO(001), which was recorded with a femtosecond laser at 4.66 eV. It reveals an apparent domain wall width of 160 nm, as is demonstrated in Fig. 6(b). Note that the intrinsic domain wall width is expected to be in the range between 60 and 210 nm as has been reported for 90° and 180° domain walls, respectively [40–42]. This experimental resolution is primarily limited by the instrumental performance of the PEEM instrument. However, for magnetic contrast it might be further reduced due to the off-axis electron detection geometry inherent to dark-field imaging. The total acquisition times for the 2D magnetic contrast images shown in Figs. 2–4 were 400, 400, and 200 s, respectively.

VII. SUMMARY AND PROSPECTS

This study demonstrates that in-plane magnetic domains can be imaged with high contrast using threshold PEEM with momentum selection of the detected photoelectrons, thereby introducing the concept of dark-field threshold MCD PEEM. We validated this approach by applying dark-field UV PEEM to an in-plane magnetized Fe(001) surface. However, this method is broadly applicable and can be extended to other ferromagnetic materials, including those with out-of-plane magnetization [17], making it well suited for investigating magnetic reorientation transitions, such as those observed in Ni/Cu(001) [13,17,43,44].

The most promising potential of this technique lies in its ability to investigate ultrafast magnetization dynamics using femtosecond laser pulses in an optical pump and a threshold UV photoemission probe scheme. This capability opens different avenues for studying the ultrafast motion of domain walls [45] or of large skyrmions on nanometer length scales [46–48].

ACKNOWLEDGMENTS

The authors thank R. Feder for fruitful discussions. We gratefully acknowledge the financial support by the Deutsche Forschungsgemeinschaft (DFG, German Research Foundation) – Project-ID 328545488 – TRR 227, Projects A06 and B04.

[1] S. Yoshida, Y. Aizawa, Z.-h. Wang, R. Oshima, Y. Mera, E. Matsuyama, H. Oigawa, O. Takeuchi, and H. Shigekawa, Probing ultrafast spin dynamics with optical pump–probe scanning tunnelling microscopy, Nat. Nanotechnol. **9**, 588 (2014).

[2] M. Müller, Imaging surfaces at the space–time limit: New perspectives of time-resolved scanning tunneling microscopy for ultrafast surface science, Prog. Surf. Sci. **99**, 100727 (2024).

[3] C. Roelcke, L. Z. Kastner, M. Graml, A. Biereder, J. Wilhelm, J. Repp, R. Huber, and Y. A. Gerasimenko, Ultrafast atomic-scale scanning tunnelling spectroscopy of a single vacancy in a monolayer crystal, Nat. Photonics **18**, 595 (2024).

[4] N. Rubiano da Silva, M. Möller, A. Feist, H. Ulrichs, C. Ropers, and S. Schäfer, Nanoscale mapping of ultrafast magnetization dynamics with femtosecond Lorentz microscopy, Phys. Rev. X **8**, 031052 (2018).

[5] M. Möller, J. H. Gaida, S. Schäfer, and C. Ropers, Few-nm tracking of current-driven magnetic vortex orbits using ultrafast Lorentz microscopy, Commun. Phys. **3**, 36 (2020).

[6] P. Tengdin, B. Truc, A. Sapozhnik, L. Kong, N. del Ser, S. Gargiulo, I. Madan, T. Schönenberger, P. R. Baral, P. Che, A. Magrez, D. Grundler, H. M. Rønnow, T. Lagrange, J. Zang, A. Rosch, and F. Carbone, Imaging the ultrafast coherent control of a skyrmion crystal, Phys. Rev. X **12**, 041030 (2022).

[7] W. Kuch, R. Schäfer, P. Fischer, and F. Hillebrecht, *Magnetic Microscopy of Layered Structures*, Springer Series in Surface Sciences Vol. 57 (Springer, Berlin, 2015).

[8] D. Kutnyakhov, R. P. Xian, M. Dendzik, M. Heber, F. Pressacco, S. Y. Agustsson, L. Wenthaus, H. Meyer, S. Gieschen, G. Mercurio, A. Benz, K. Bühlman, S. Däster, R. Gort, D. Curcio, K. Volckaert, M. Bianchi, C. Sanders, J. A. Miwa, S. Ulstrup *et al.*, Time- and momentum-resolved photoemission studies using time-of-flight momentum microscopy at a free-electron laser, Rev. Sci. Instrum. **91**, 013109 (2020).

[9] G. K. L. Marx, H. J. Elmers, and G. Schönhense, Magneto-optical linear dichroism in threshold photoemission electron microscopy of polycrystalline Fe films, Phys. Rev. Lett. **84**, 5888 (2000).

[10] C. M. Schneider, M. S. Hammond, P. Schuster, A. Cebollada, R. Miranda, and J. Kirschner, Observation of magnetic circular dichroism in UV photoemission from ferromagnetic fcc cobalt films, Phys. Rev. B **44**, 12066 (1991).

[11] J. Henk, T. Scheunemann, S. V. Halilov, and R. Feder, Magnetic dichroism and electron spin polarization in photoemission: Analytical results, J. Phys.: Condens. Matter **8**, 47 (1996).

[12] R. Feder and J. Henk, Magnetic dichroism and spin polarization in valence band photoemission, in *Spin-Orbit-Influenced Spectroscopies of Magnetic Solids*, edited by H. Araki, E. Brézin, J. Ehlers, U. Frisch, K. Hepp, R. L. Jaffe, R. Kippenhahn, H. A. Weidenmüller, J. Wess, J. Zittartz, W. Beiglböck, H. Ebert, and G. Schütz, Lecture Notes in Physics Vol. 466 (Springer, Berlin, 1996), p. 85.

[13] T. Nakagawa and T. Yokoyama, Magnetic circular dichroism near the Fermi level, Phys. Rev. Lett. **96**, 237402 (2006).

[14] T. Nakagawa, T. Yokoyama, M. Hosaka, and M. Katoh, Measurements of threshold photoemission magnetic dichroism using ultraviolet lasers and a photoelastic modulator, Rev. Sci. Instrum. **78**, 023907 (2007).

[15] T. Nakagawa, K. Watanabe, Y. Matsumoto, and T. Yokoyama, Magnetic circular dichroism photoemission electron microscopy using laser and threshold photoemission, J. Phys.: Condens. Matter **21**, 314010 (2009).

[16] T. Nakagawa and T. Yokoyama, Laser induced threshold photoemission magnetic circular dichroism and its application to photoelectron microscope, J. Electron Spectrosc. Relat. Phenom. **185**, 356 (2012).

[17] M. Kronseder, J. Minár, J. Braun, S. Günther, G. Woltersdorf, H. Ebert, and C. H. Back, Threshold photoemission magnetic circular dichroism of perpendicularly magnetized Ni films on Cu(001): Theory and experiment, Phys. Rev. B **83**, 132404 (2011).

[18] T. N. G. Meier, M. Kronseder, and C. H. Back, Domain-width model for perpendicularly magnetized systems with Dzyaloshinskii-Moriya interaction, Phys. Rev. B **96**, 144408 (2017).

[19] Y. Zhao, H. Lyu, G. Yang, B. Dong, J. Qi, J. Zhang, Z. Zhu, Y. Sun, G. Yu, Y. Jiang, H. Wei, J. Wang, J. Lu, Z. Wang, J. Cai, B. Shen, W. Zhan, F. Yang, S. Zhang, and S. Wang, Direct observation of magnetic contrast obtained by photoemission electron microscopy with deep ultra-violet laser excitation, Ultramicroscopy **202**, 156 (2019).

[20] E. Tamura, W. Piepke, and R. Feder, New spin-polarization effect in photoemission from nonmagnetic surfaces, Phys. Rev. Lett. **59**, 934 (1987).

[21] W. Kuch, A. Dittschar, K. Meinel, M. Zharnikov, C. M. Schneider, J. Kirschner, J. Henk, and R. Feder, Magnetic-circular-dichroism study of the valence states of perpendicularly magnetized Ni(001) films, Phys. Rev. B **53**, 11621 (1996).

[22] R. Feder, J. Henk, and B. Johansson, Magnetic dichroism in threshold photoemission, Solid State Commun. **108**, 713 (1998).

[23] D. Venus, Interrelation of magnetic-dichroism effects seen in the angular distribution of photoelectrons from surfaces, Phys. Rev. B **49**, 8821 (1994).

[24] D. Venus, Interpretation of magnetic dichroism in angle-resolved UV photoemission from valence bands, J. Magn. Magn. Mater. **170**, 29 (1997).

[25] W. Kuch and C. M. Schneider, Magnetic dichroism in valence band photoemission, Rep. Prog. Phys. **64**, 147 (2001).

[26] D. Venus, W. Kuch, A. Dittschar, M. Zharnikov, C. M. Schneider, and J. Kirschner, Spin-dependent surface transmission in 3*d* metals: Implications for magnetic-dichroism measurements of the valence bands, Phys. Rev. B **52**, 6174 (1995).

[27] K. Hild, J. Maul, T. Meng, M. Kallmayer, G. Schönhense, H. J. Elmers, R. Ramos, S. K. Arora, and I. V. Shvets, Optical magnetic circular dichroism in threshold photoemission from a magnetite thin film, J. Phys.: Condens. Matter **20**, 235218 (2008).

[28] K. Hild, J. Maul, G. Schönhense, H. J. Elmers, M. Amft, and P. M. Oppeneer, Magnetic circular dichroism in two-photon photoemission, Phys. Rev. Lett. **102**, 057207 (2009).

[29] K. Hild, G. Schönhense, H. J. Elmers, T. Nakagawa, T. Yokoyama, K. Tarafder, and P. M. Oppeneer, Energy- and angle-dependent threshold photoemission magnetic circular dichroism from an ultrathin Co/Pt(111) film, Phys. Rev. B **82**, 195430 (2010).

[30] J. Henk and B. Johansson, Magnetic dichroism in off-normal valence-band photoemission, J. Electron Spectrosc. Relat. Phenom. **94**, 259 (1998).

[31] C. Tusche, M. Ellguth, V. Feyer, A. Krasyuk, C. Wiemann, J. Henk, C. M. Schneider, and J. Kirschner, Nonlocal electron correlations in an itinerant ferromagnet, Nat. Commun. **9**, 3727 (2018).

[32] J. Henk, W. Schattke, H. Carstensen, R. Manzke, and M. Skibowski, Surface-barrier and polarization effects in the photoemission from GaAs(110), Phys. Rev. B **47**, 2251 (1993).

[33] K. Duncker, M. Kiel, and W. Widdra, Momentum-resolved lifetimes of image-potential states on Ag(001), Surf. Sci. **606**, L87 (2012).

[34] K. Gillmeister, D. Golež, C.-T. Chiang, N. Bittner, Y. Pavlyukh, J. Berakdar, P. Werner, and W. Widdra, Ultrafast coupled charge and spin dynamics in strongly correlated NiO, Nat. Commun. **11**, 4095 (2020).

[35] M. Paleschke, C.-T. Chiang, L. Brandt, N. Liebing, G. Woltersdorf, and W. Widdra, Plasmonic spin-Hall effect of propagating surface plasmon polaritons in $Ni_{80}Fe_{20}$ microstructures, New J. Phys. **23**, 093006 (2021).

[36] F. O. Schumann, M. Paleschke, J. Henk, W. Widdra, and C.-T. Chiang, Improved imaging of magnetic domains with a photoelectron emission microscope by utilizing symmetry and momentum selection, arXiv:2505.17658.

[37] K. Gillmeister, M. Kiel, and W. Widdra, Image potential states at transition metal oxide surfaces: A time-resolved two-photon photoemission study on ultrathin NiO films, Phys. Rev. B **97**, 085424 (2018).

[38] B. Krömker, M. Escher, D. Funnemann, D. Hartung, H. Engelhard, and J. Kirschner, Development of a momentum microscope for time resolved band structure imaging, Rev. Sci. Instrum. **79**, 053702 (2008).

[39] M. Kotsugi, W. Kuch, F. Offi, L. I. Chelaru, and J. Kirschner, Microspectroscopic two-dimensional Fermi surface mapping using a photoelectron emission microscope, Rev. Sci. Instrum. **74**, 2754 (2003).

[40] J. Lee, M. Dreyer, C. Krafft, and R. Gomez, Scanning tunneling microscopy/magnetic force microscopy study of ultrathin Fe film on MgO(001) in ultrahigh vacuum, J. Appl. Phys. **101**, 09D123 (2007).

[41] H. P. Oepen and J. Kirschner, Magnetization distribution of 180° domain walls at Fe(100) single-crystal surfaces, Phys. Rev. Lett. **62**, 819 (1989).

[42] M. Escher, N. B. Weber, T.-J. Kühn, and M. Patt, 2D imaging spin-filter for NanoESCA based on Au/Ir(001) or Fe(001)-p(1 × 1)O, Ultramicroscopy **253**, 113814 (2023).

[43] J. Henk, A. M. N. Niklasson, and B. Johansson, Magnetism and anisotropy of ultrathin Ni films on Cu(001), Phys. Rev. B **59**, 9332 (1999).

[44] D. Sander, W. Pan, S. Ouazi, J. Kirschner, W. Meyer, M. Krause, S. Muller, L. Hammer, and K. Heinz, Reversible H-induced switching of the magnetic easy axis in Ni/Cu(001) thin films, Phys. Rev. Lett. **93**, 247203 (2004).

[45] S. S. P. Parkin, M. Hayashi, and L. Thomas, Magnetic domain-wall racetrack memory, Science **320**, 190 (2008).

[46] B. Göbel, A. F. Schäffer, J. Berakdar, I. Mertig, and S. S. P. Parkin, Electrical writing, deleting, reading, and moving of magnetic skyrmioniums in a racetrack device, Sci. Rep. **9**, 12119 (2019).

[47] H. Jani, J.-C. Lin, J. Chen, J. Harrison, F. Maccherozzi, J. Schad, S. Prakash, C.-B. Eom, A. Ariando, T. Venkatesan, and P. G. Radaelli, Antiferromagnetic half-skyrmions and bimerons at room temperature, Nature (London) **590**, 74 (2021).

[48] L.-M. Kern, B. Pfau, V. Deinhart, M. Schneider, C. Klose, K. Gerlinger, S. Wittrock, D. Engel, I. Will, C. M. Günther, R. Liefferink, J. H. Mentink, S. Wintz, M. Weigand, M.-J. Huang, R. Battistelli, D. Metternich, F. Büttner, K. Höflich, and S. Eisebitt, Deterministic generation and guided motion of magnetic skyrmions by focused He^+-ion irradiation, Nano Lett. **22**, 4028 (2022).